# Nanoplastic Flows of Glassy Polymer Chains Interacting with Multiwalled Carbon Nanotubes in Nanocomposites

**C.-W. Lin,[†] L. C. Huang,[†] C.-C. M. Ma,[‡] A. C.-M. Yang,*[,†] C.-J. Lin,[§] and L.-J. Lin[§]**

*Department of Materials Science and Engineering, and, Department of Chemical Engineering, National Tsing Hua University, Hsinchu, Taiwan, Materials Research Laboratories, Industrial Technology Research Institute, Hsinchu, Taiwan*

*Received October 22, 2007; Revised Manuscript Received April 23, 2008*

ABSTRACT: Interactions between glassy polymer chains and the uniformly dispersed carbon nanotubes (CNTs) in nanocomposites were investigated with surface-grafted multiwalled CNTs dispersed in two model polymer systems, polystyrene (PS) and poly(phenylene oxide) (PPO), representing respectively brittle and ductile polymers. Although significant mechanical reinforcement in the both systems was observed, drastically different microscopic interactions, engendered from variations in the fundamental behavior of entangled chains, were noted during the nanoplastic flow of crazing or shear yielding in the nanocomposites. As revealed by a local stress analysis based on atomic force microscopy, "extensibility" of the entanglement network determines not only the mode of deformation leading to either crazing or shear yielding but also how the stretched chains interact with individual nanotubes. The results bear important implications on our understanding toward the fundamental behavior of entangled macromolecules in the glassy state.

## Introduction

The nanocomposites based on well-dispersed carbon nanotubes (CNTs) embedded in carefully selected polymer matrices have increasingly attracted attention due to their great potentials for innovative mechanical, electrical, thermal, and optoelectronic properties. The outstanding advantageous properties of CNTs, such as the exceedingly high Young's modulus[1,2] and conductivities[3,4] and large flexibility limits and fracture strains,[5] and the simple fact that they are tiny tubules with extremely high aspect ratios have made CNT an ideal filler for most polymers. In this context, the interactions between the embedded CNTs and the surrounding polymer chains not only are very interesting in the light of unveiling the fundamental chain behavior of the entangled macromolecules. They however also are of vital importance due to requirement of controllable CNT−polymer interactions down to the nanometer scales for successful modification of the physical properties.

Previous work on CNTs as fillers in polymers has been focused primarily on the low-strain elastic behavior and cracking properties.[6−15] Little attentions had been paid to the more important plastic flows regime that constitutes the major part of the mechanical performance before fracture. The elastic modulus and breaking stress in polystyrene (PS) were shown by Qian et al.[9,16] to increase significantly by the addition of CNTs, pointing to the significant role of load transfer of CNTs. Watts et al.[17] also identified the CNT pull-out mechanism during cracking, which effectively retarded the fracture in the CNTs−PS thin films. Apparently, observations of the CNT effects on stress transfer or failure processes strongly depend on the state of CNT dispersion and their interactions with the polymer chains. Moreover, given the above-mentioned reinforcement effects, it is disappointing to observe that the optimal CNT reinforcement results were always observed in the regime of a small CNT fractions (∼1−2 wt %)[10,13,18−20] while the properties, like that caused by most other fillers beyond a percolation threshold, fell off considerably for higher CNTs loadings (>5 wt %).[11,21] It indicates the necessity of more in-depth investigation of the CNT−polymer interactions over a wider range of deformation that includes both the elastic and plastic behavior.

It is well-known that glassy polymers develop microscopic deformation zones of crazes[22−35] or shear deformation zones (SDZs)[22,25,27,32] before fracture (Figure 1, parts a and b). The stress-induced local plastic flow that gives rise to the formation of these microscopic deformation zones triggers extraordinarily large plastic strains (∼200−300%) within the deformation zones and is the basic molecular mechanism for yielding in most glassy polymers. The occurrence of crazes or SDZs depends on the entanglement density $\nu_e$ of the polymer matrix.[22,30−32,34] In addition, crazing and shear yielding represent respectively the precursor of brittle and ductile fracture of glassy polymers. They are both produced by micronecking induced during the plastic flow,[33−35,37,39] but the microstructures are quite different in that crazes are constructed by interconnected fibrils embedded in voids while SDZs are microscopically thinned smooth regions (Figure 1).[22,25,28−32,34,36,39] The diameters of the craze fibrils are in the range of 6−20 nm, thus the local deformations are deemed to be nanoplastic flows. The microscopic reinforcement mechanisms of CNTs in glassy polymers should lie in the CNT interactions with these nanoplastic flows.

Previously, the role of multiwalled CNTs (MWCNTs) during crazing in PS-CNTs nanocomposites was explored[38,39] and strain delocalization was identified to be the origin of fracture toughness enhancement. In these nanocomposites, most CNTs were observed to be excluded from crazes. In this study, more thorough investigation of the interactions between MWCNTs and polymer chains was undertaken by further examining the MWCNTs reinforcement in PS and in the SDZ-forming poly(phenylene oxide) (PPO). The work has led to a more complete and coherent scenario of the interactions between CNTs and polymer chains that satisfactorily explains reinforcement due to CNTs. The role of entanglement chain network during plastic flow in the nanocomposite was also unveiled, which sheds important light on the fundamental behavior of polymer chains in the glassy state.

* Corresponding author.
[†] Department of Materials Science and Engineering, National Tsing Hua University.
[‡] Department of Chemical Engineering, National Tsing Hua University.
[§] Materials Research Laboratories, Industrial Technology Research Institute.

10.1021/ma702342z CCC: $40.75 
Published on Web 06/11/2008

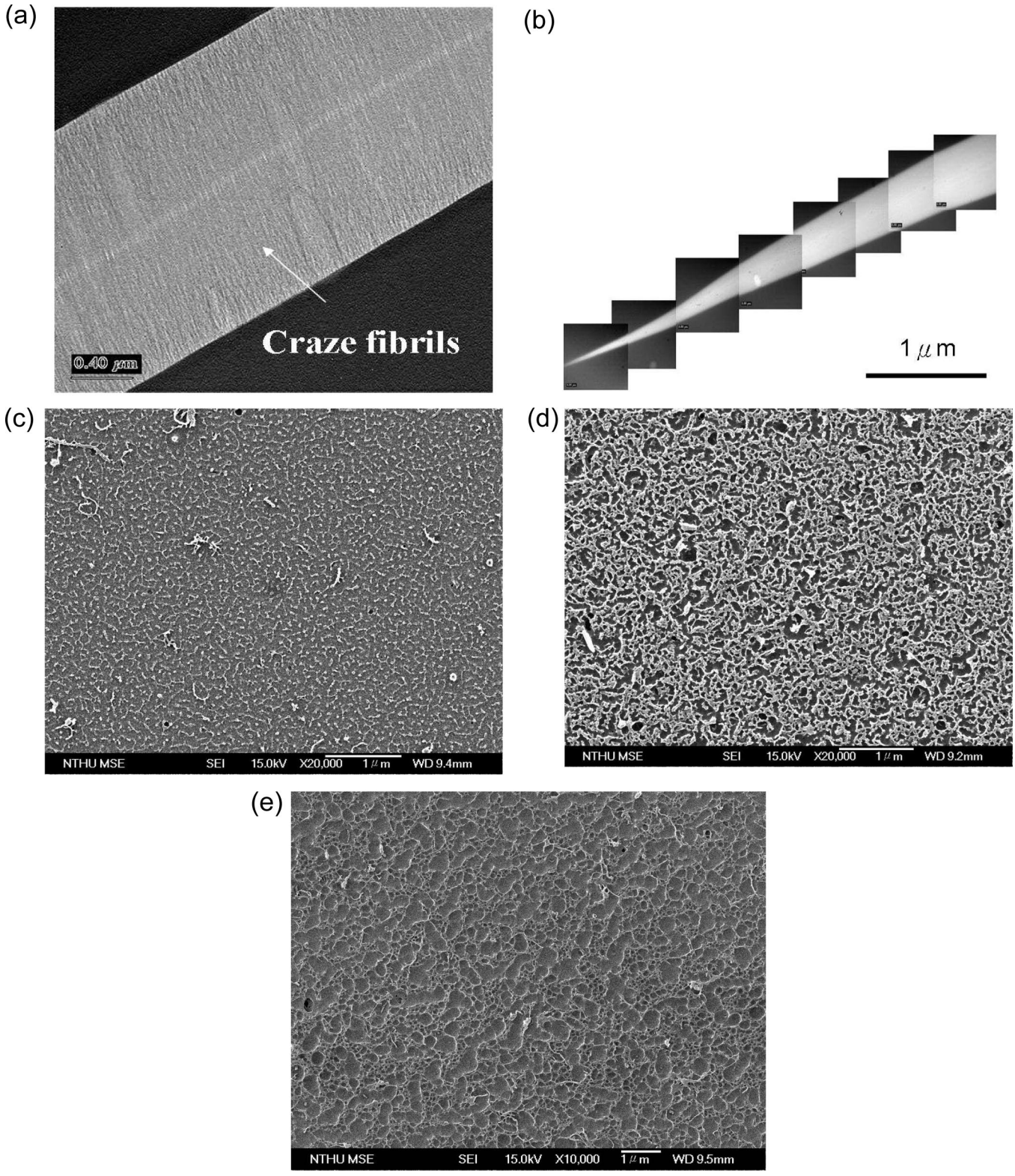


**Figure 1.** (a) a TEM micrograph of a craze in pristine PS film. (b) TEM micrograph of a shear deformation zone in pristine PPO film. (c−e) SEM micrographs of the plasma etched nanocomposites showing good CNT dispersion: (c) PS matrix with $c_0 = 2.0$ wt %; (d) PS matrix with $c_0 = 5.0$ wt %; (e) PPO matrix with $c_0 = 2.4$ wt %.

## Experimental Section

Monodisperse PS of molecular weight ($M_w$) 2000K (Pressure Chemical Co.) and PPO polymer with $M_w = 244$K (Aldrich Chemical Co.) were used as-received. The MWCNTs (DESUN Nano Co., Taiwan) for this study, as determined from TEM examinations, have an average outer diameter around 10−35 nm and a length in the range of 10−30 $\mu$m.

The method of preparing the surface-grafted MWCNTs with long PS chains (PS-*g*-MWCNTs) was reported elsewhere[38,39] and will not be re-emphasized here. The average molecular weight of the grafted PS in PS−MWCNTs was measured to be around 60K (polydisperity = 2.1) from gel permeation chromatography after the defunctionalization process.[40] As determined from thermogravimetric analysis (TGA), the weight fraction of PS in

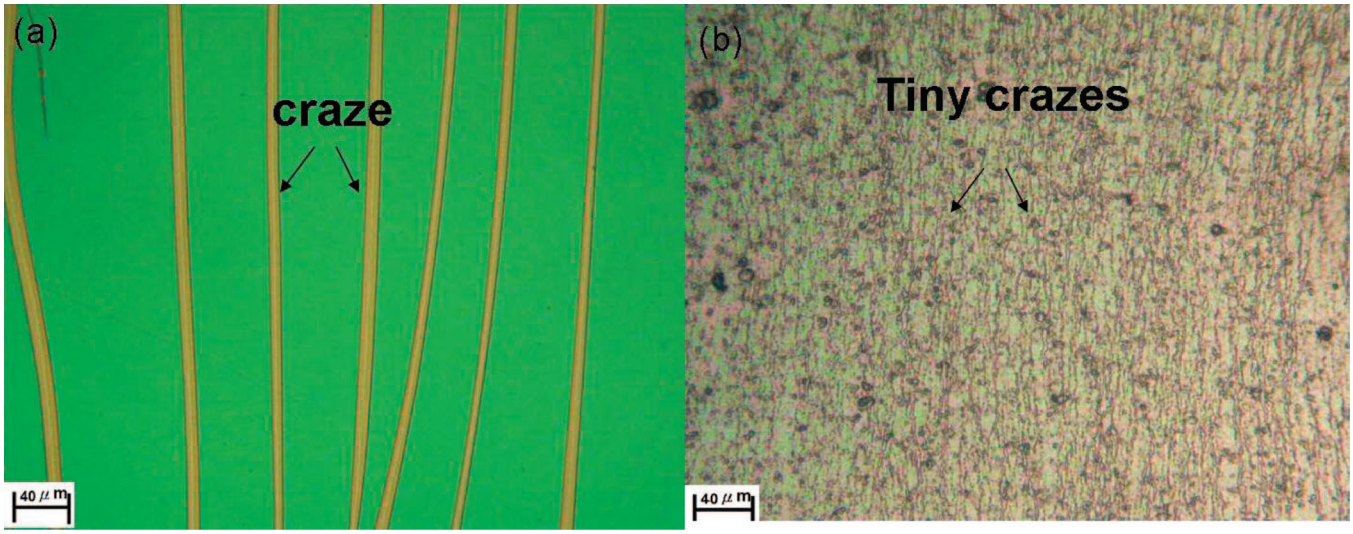


**Figure 2.** Optical micrographs of stretched (a) pristine PS films and (b) MWCNTs/PS composite film ($c_0 = 2$ wt %).

PS−MWCNTs nanocomposites is approximately 60 wt %. The average length of PS-*g*-MWCNTs is around 1−3 $\mu$m.

The grafted MWCNTs were then mixed with the neat PS (or PPO) in toluene from which thin films (MWCNTs/PS or MWCNTs/PPO) with film thickness controlled at approximately 0.5 $\mu$m were spincoated on clean glass slides from the solution. The fraction of the surface-grafted MWCNTs in the film ($c_0$) ranges from 0 to 10 wt %. The films were then transported and bonded to a supporting copper grid for mechanical experiments.[30,31,34,38]Before the mechanical testing, aging at 120 °C for 1 h was routinely carried out for MWCNTs/PPO films to enhance the strain localization required for growing SDZs.[36] During the mechanical test, the nanocomposite specimen was mounted in a strain jig, stretched under an optical microscope to observe the growth of deformation zones (crazes or SDZs).[30,31,33–35,38] The samples were then examined under an AFM (Digital Instrumental, Nanoscope IIIa) for detailed analyses of the microdeformation, including calculations of the local stress and strain in the deformation zones.[34,35] A transmission electron microscopy (TEM, JEOL JEM-2010) was used to obtain images of crazes or SDZs of the stretched samples. Taking advantage of the film-on-grid method,[30,31,34,38] a large number of crazes and SDZs were examined, enabling the presentation here of typical and highly reproducible data for reliable interpretations. Widening of the microdeformation zones was monitored by using a video camera attached to an optical microscope and from the images of the growing crazes or SDZs the widening velocities were obtained. The dispersion of MWCNTs in the polymer matrix was examined by using a field-emission scanning electron microscope (FE-SEM; xxxx) after gently etching the samples with oxygen plasma.[38,39] The dispersion of MWCNTs has been excellent, as shown in Figure 1, parts c and d, such that the mechanical performance of the nanocomposites is consistent and reproducible.

## Results

The plastic flow induced by local strains in glassy polymers gives rise to the formation of microdeformation zones. For brittle polymers such as PS, crazes arise from large local strains up to 300%, depending on the entanglement density.[22,30–32] On the other hand, PPO, a model system for ductile glassy polymers, develops SDZ resulted from local strain around 100% upon application of stresses. According to Kramer's ground-breaking work, the line of demarcation between the brittle and the ductile behaviors can be defined by a critical entanglement density $\nu_e^c$ such that when $\nu_e > \nu_e^c$ (tight networks) shear deformation zones prevails, while crazes dominate in the regime of $\nu_e < \nu_e^c$ (loose networks). Under ambient conditions, $\nu_e^c \sim 6 \times 10^{25}/m^3$.[22,25,27] As will be shown later, the "tightness" of the chain entanglement networks determines not only whether the glassy polymer behaves in a ductile or brittle way, but also how the imbedded MWCNTs interact with the polymer chains during the plastic flow in the deformed glass.

**Crazes Morphology.** In the pristine PS films, crazes initiated at approximation 1% strain ($\epsilon$) and they were generally straight, widening steadily as the strain increased, and the maximum width of creases could reach approximately 20 $\mu$m (Figure 2a). Local fibril breakdowns within the crazes started at approximately $\epsilon = 8\%$. Craze surface topography determined from AFM revealed that craze depth $d$ increased almost linearly with craze width $w$ when $w < w_c$ (see, for example, Figure 28 of ref 38). The critical width $w_c$ is a function of film thickness (for 0.5 $\mu$m thick PS film, $w_c \sim 2.5$ $\mu$m) and representing the start of the microneck propagation.[33–35,38,39] For $w > w_c$, craze depth became constant with $w$, indicating steady-state drawing of the crazing plastic flow.

The films of the MWCNTs/PS composites with MWCNTs content ($c_0$) of 2 wt % demonstrated a quite different mechanical behavior in that the crazes were generally short and narrow (mostly less than 2 $\mu$m wide) and no cracking was observed even at strains greater than 20% (Figure 2b). Moreover, although the craze depth $d$ varied with craze width $w$ following the same curve as that of pristine PS, $w$ never reached $w_c$.[38,39] It indicates that the micronecking characteristic of crazing was not altered by the presence of MWCNTs, however, the process was strongly suppressed. For films contain MWCNTs less than 1wt %, the observed effect due to MWCNTs on the microscopic deformation behavior was not obvious and no qualitative variations from that observed in films of $c_0 = 2$ wt % were noted.

From AFM craze topography, the MWCNTs/PS nanocomposites evidently developed a concentrated plastic strain within the craze (Figure 3a, for $c_0 = 2$ wt%) with the maximum strain $\epsilon_p$ within the craze increasing with $w$ but eventually leveling off for $w < 1$ $\mu$m. This is similar to the behavior of the pristine PS.[33–35,38,39,41–43] Note that for narrow crazes ($w > 0.6$ $\mu$m), $\epsilon_p$ is just below 30%, a value very close to the reported elastic limit of carbon nanotubes.[5] Figure 4a shows a TEM micrograph of a craze tip propagating into a region of densely populated MWCNTs. The presence of the MWCNTs seems to have no effect on the growth of the craze in that the craze tip penetrates right through the MWCNTs. Since $\epsilon_p$ in the narrow crazes is below the elastic limit of MWCNTs, the MWCNTs within them

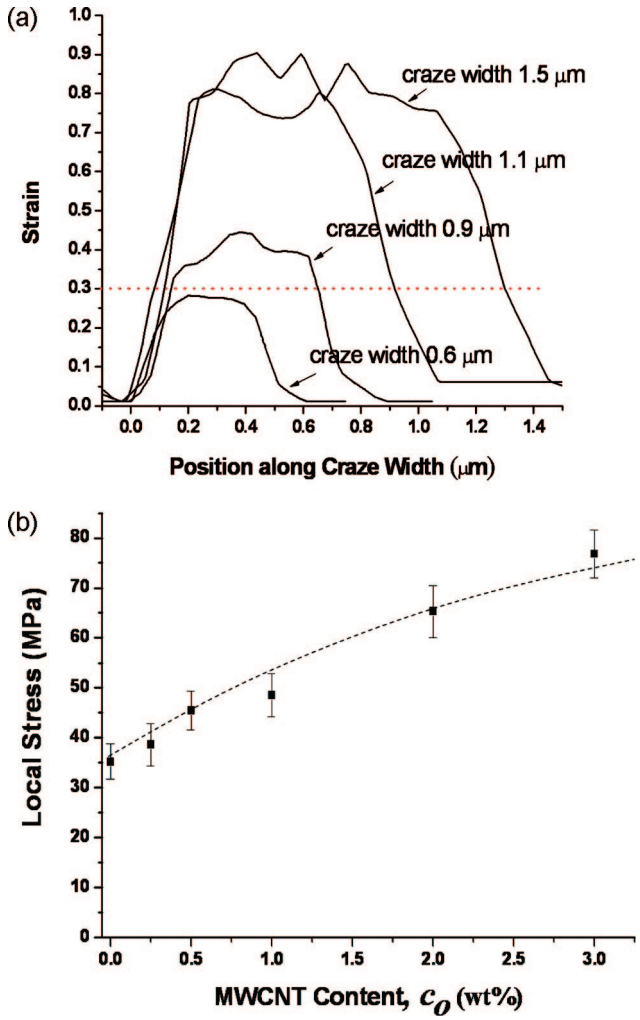


**Figure 3.** (a) Local strain distribution within a craze across the craze width for $c_0 = 2$ wt %, and (b) local stress within MWCNT/PS films with $c_0$ (for $w = 0.7$ $\mu$m).

thus can easily survived without inflicting breakage of the MWCNTs or being forced to substantially modify the plastic flow process.

In contrast, only of very rare incidence were intact MWCNTs observed within wider crazes. Generally, when craze width exceeds certain limit only broken pieces of MWCNTs were observed within the craze (Figure 4, parts b and c). Later examinations revealed that this width limit corresponds to that above which the local strain becomes significant in comparison to the extension limit of MWCNTs. The intact MWCNTs in the wider crazes were either incorporated from craze tips or from fibrillation of the "film" islands within crazes, which were formed by the merging of locally parallel crazes to traps intact MWCNTs within the new crazes. It seems quite unlikely for the plastic-flowed PS chains to pull MWCNTs across the craze boundaries into the microdeformation zones. Most MWCNTs embedded in the PS matrix appeared to stay outside the crazes. For those MWCNTs incorporated within crazes, depending on the drawing history, they were subject to different degree of stretching. Some were broken, leaving broken ends at the boundaries (Figure 4c). The local stresses within crazes in the films determined from AFM topography were in the order of 150 MPa. Since they were significantly less than the fracture stress of CNTs, the breakages of MWCNTs were likely to have occurred at the defects sites induced during surface treatments. Moreover, in the wider crazes ($w < 0.6$ $\mu$m) the plateau plastic strain $\epsilon_p$ (Figure 3a) had exceeded the flexibility limit of MWCNTs, hence either forced breakage or stress-shielding of the surrounding by the incorporated MWCNTs would occur. The latter should lead to a constraint craze widening, but it only played a minor role due to the insignificant number of MWCNTs within crazes.

The exclusion of MWCNTs from crazing process was confirmed by AFM topography of the crazed films dry-etched by mild oxygen plasma,[38] of which protrusions arising from pileup of the slow-etched MWCNTs were observed bulging along the craze boundaries. The protrusion width, $w_p$, was determined by first measuring the apparent width of the protrusions as a function of etching time (inset of Figure 5a), and then the level-off value was taken as the protrusion width. The protrusion width was found to increase with craze width (Figure 5a). Correspondingly, the height of the protrusions was also found to increase with craze width, from 60 to 120 nm for $w_p$ varying from 210 to 320 nm. This is consistent with the TEM observations (Figure 5b) that MWCNTs are excluded from crazes during fibrillation, engendering greater concentrations of MWCNTs at boundaries of the wider crazes.

**Fibrillation Modified by MWCNTs.** The local concentration of MWCNTs at craze boundaries was calculated, from the AFM data, to assess quantitatively how craze fibrillation was modified by the pileup of MWCNTs. Assuming all the MWCNTs in the course of craze widening would be excluded from crazes fibrillation, the local concentration of MWCNTs at craze boundaries ($c_{pu}$) can be readily shown to depend on the original concentration of MWCNTs ($c_0$) in the film, the craze width ($w$), protruding width ($w_p$), the film thickness at the craze ($\tau_c$), mass densitny of craze ($\rho = 0.8$ g/cm$^3$), and the original film thickness ($\tau_0$), as

$$c_{pu} = c_0(1 + w\rho\tau_c/2w_p\tau_0) \quad (1)$$

Obviously, eq 1 applies only for the regime where the wide crazes effectively exclude MWCNTs from the nanoplastic flow. Figure 5c indicates that $c_{pu}$ increased approximately linearly with craze width $w$. The slope, increasing with $c_0$, is quite steep. For a 2 $\mu$m wide craze, for example, $c_{pu}$ goes up four times to 8 wt % in films of $c_0 = 2$ wt %. It indicated that the PS chains to be drawn across the craze boundaries need to pass through an increasingly denser network of MWCNTs at the boundaries. Thus, a greater drawing stress will be required for the PS chains to overcome the increasing chain frictions with the MWCNTs, and hence craze widening becomes more and more difficult. This ultimately enhances delocalization of the plastic flow of crazing.

The increase of chain friction due to MWCNTs was estimated using a Rouse tube model.[44] During the nanoplastic flow process of a glassy polymer, the chain pulled by the necking force $f$ was assumed to undergo a constant sliding velocity $v$ along the "topological tube" defined by the entangled chains, where $f$ and $v$ are related via the total frictional coefficient $\zeta_R$ of the whole chain, as

$$f = v\zeta_R \quad (2)$$

The pulling force $f$ can be determined from the drawing stress $\sigma$ during crazing and the cross-sectional area of the chain $A_{chain}$ by $f = \sigma A_{chain}$. The cross-sectional area $A_{chain}$ is approximately 0.688 nm$^2$ for a single PS chain in the tube where a total of 22 in average share the tube space.[44,45]

For pristine PS films, the pulling force $f$ was calculated to be $f = 0.065$ nN corresponding to the steadily state necking stress $\tau = 94$ MPa determined from AFM results.[34,35] The chain sliding velocity $v$ was calculated from the craze widening speed, measured from video camera, at steady-state necking, which

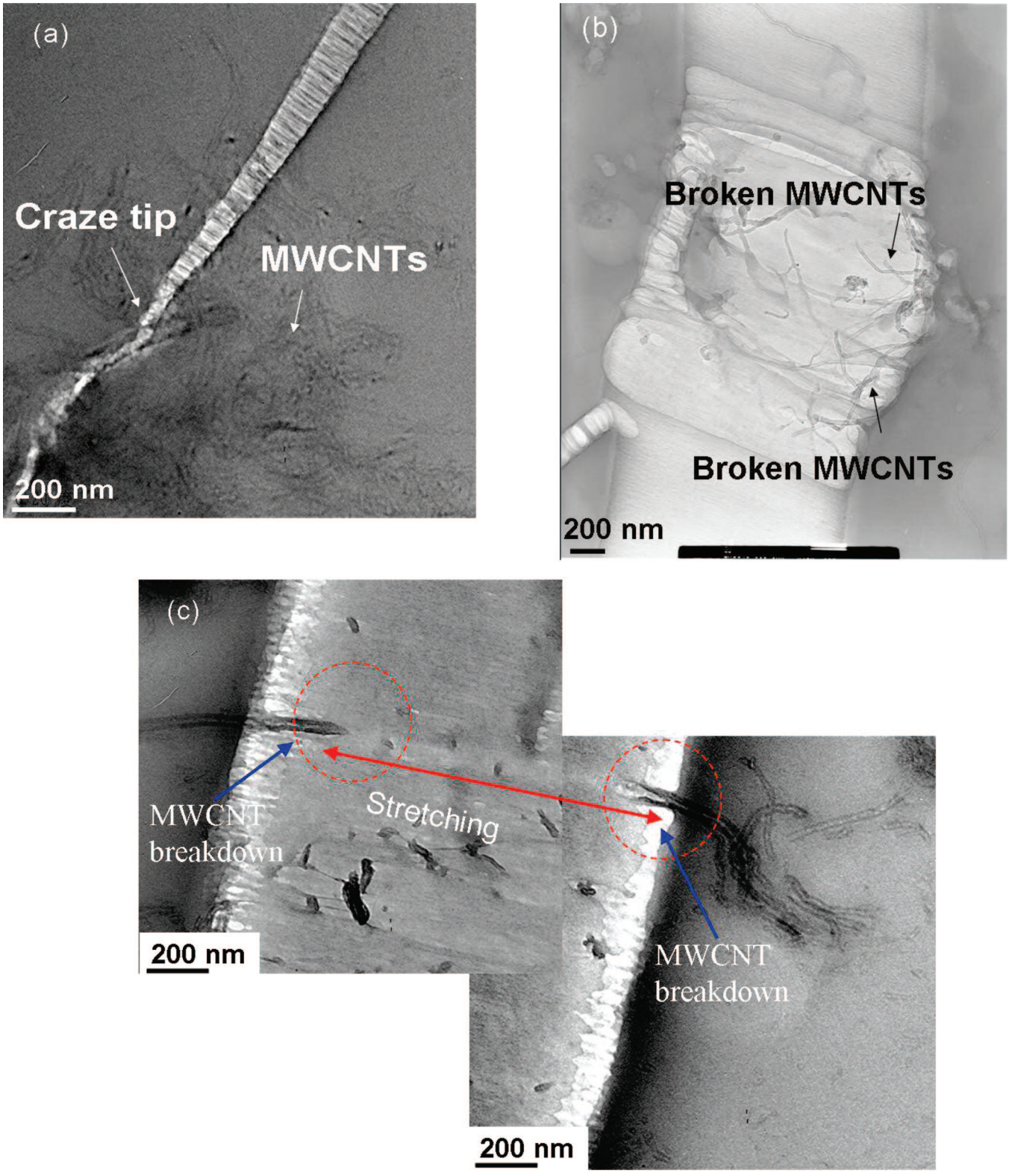


**Figure 4.** TEM micrographs of (a) a craze tip, (b) wider craze in MWCNT/PS films ($c_0 = 2$ wt %), and (c) fracture of nanotubes in MWCNT/PS films ($c_0 = 2$ wt %).

was then corrected by a factor of $N^{1/2}$ where $N$ is the number of Kuhn monomer in the tube to take into account of the random coil chain conformation.[44,46] For PS of $M_w = 2000$K, $N$ is approximately 2800 (Kuhn monomer molar mass: 720 g/mol.). The craze widening velocity $v$ was measured to be approximately 140 nm/s, the chain sliding velocity $v$ thus is determined to be approximately 7400 nm/s. As shown in Figure 5d, $v$ decreases slightly with craze widening until it levels as $w$ passes the critical width $w_c$. The decrease obviously is due to strain hardening during the micronecking. From eq. 2, the friction coefficient of PS chain ($\zeta_{PS}$) in the pristine polymer was calculated and found to be dependent on $w$. In the steady-state necking regime, $\zeta_{PS} = 1.13 \times 10^{-5}$ kg/s was obtained (Figure 5e).

For the MWCNT/PS films, MWCNT pileup at craze boundaries increases the chain frictional force during the

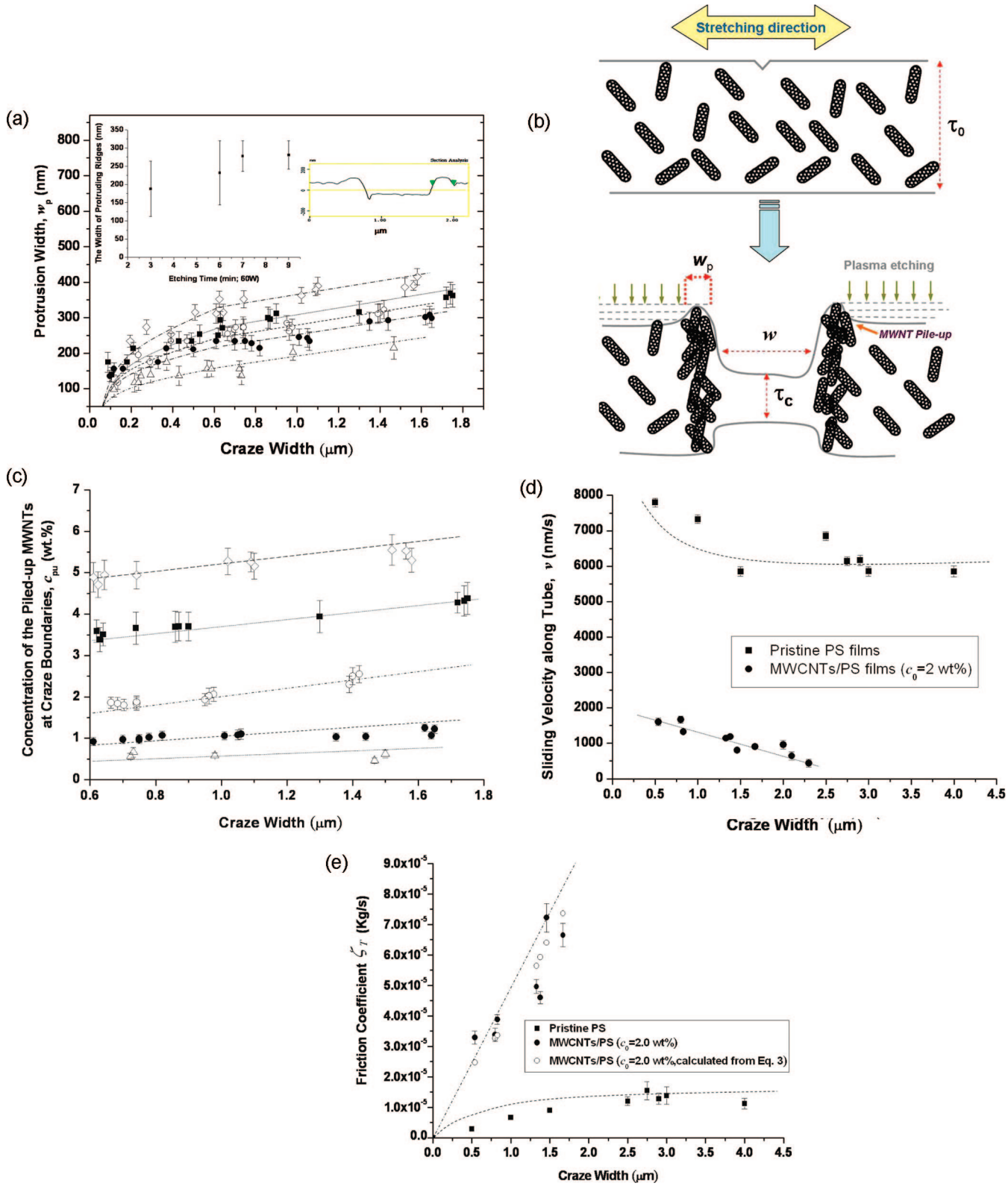


**Figure 5.** (a) Width of MWCNT pile-up at craze boundaries versus craze width, $c_0 = 3.0$ wt % ($\zeta_0 = 2.0$ wt % ($\zeta_0 = 1.0$ wt % ($\zeta_0 = 0.5$ wt % ($\zeta_0 = 0.25$ wt % ($\epsilon$). Insets: The width of the MWCNT pileup at the craze boundaries determined by AFM topographic profile and shown as a function of etching time, (b) a schematic of the MWCNT piled up at the craze boundaries, (c) the weight percentage of MWCNT protruding vs width of craze in MWNT/PS films, $c_0 = 3.0$ wt % ($\epsilon$); $c_0 = 2.0$ wt % ($\zeta c_0 = 1.0$ wt % ($\zeta$; $c_0 = 0.5$ wt % ($\zeta$; $c_0 = 0.25$ wt % ($\epsilon$), (d) tube sliding velocity of a PS chain versus craze width in pristine PS and MWCNT/PS films, and (e) the friction coefficient of a PS chain versus craze width in pristine PS and MWCNT/PS films.

nanoplastic flow. The friction coefficient $\zeta_T$ associated with a sliding chain going through a mixture of semidilute MWCNTs concentrations in PS where PS-CNT interactions dominate, can be described in terms of the number of nanotubes per volume $v_{pu}$ and the MWCNT geometries (length $l_{cnt}$ and diameter $d_{cnt}$) as

$$\varsigma_T = \varsigma_{PS}\left(1 + \frac{\pi}{30\beta}\frac{(\nu_{Pu} i_{cnt}^{\ 3})^3}{in\left(\frac{i_{cnt}}{d_{cnt}}\right)}\right) \quad (3)$$

where $\beta$ is a numerical factor ($\beta = 1.32 \times 10^3$).[47,48] This equation was originally developed[47] for the rheological behavior of CNTs/polymer nanocomposites by simulating the nanocomposite as one that contains rodlike particles in a matrix. Moreover, for the sake of simplicity, the chain conformation in the MWCNTs/PS systems is assumed to be approximately the same as that in pristine PS such that the length and molar mass of the Kuhn monomer remain unchanged. Using eq 3, the chain friction $\zeta_T$ during the nanoplastic flow can be calculated from $c_{pu}$, measured from AFM, and the nanotube geometrical constants ($l_{cnt} = 1.4$ $\mu$m, $d_{cnt} = 35$ nm). As shown in Figure 5e, $\zeta_T$ increased almost linearly with craze width $w$ for $0 < w < 2.0$ $\mu$m. Within the same craze width range, the chain sliding velocity $v$, readily obtained from $\zeta_T$ and the necking force $f$ (from AFM stress analysis) using eq 2 (Figure 5d), was found to decrease steadily as craze widened, and for $w > 2.5$ $\mu$m, $v$ became approximately zero, consistent with experimental observations that virtually all crazes in the MWCNTs/PS films were narrower than 2 $\mu$m. The chain friction during the nanoplastic flow can also be obtained directly from craze widening measured by video taping using eq 2. The frictional coefficient $\zeta_T$ so-obtained was found in excellent agreement with that determined based on MWCNT pileup ($c_{pu}$) at craze boundaries (Figure 5e). This result strongly supports that the pileup of MWCNTs at craze boundaries caused an increase in chain friction, thus restricted the widening of existing crazes, forcing new craze initiation in the other regions to absorb the applied strain.

**Embrittlement Induced by MWCNTs.** The exclusion of MWCNTs from the nanoplastic flow had increased the difficulty of chain fibrillation and forced a competition between initiation of new crazes and widening of the existing crazes, leading to a substantial reduction in craze widths. Since the probability of craze breakdown increases exponentially with craze width,[30–32] delocalization of crazing reinforced the mechanical stability of the nanocomposite. Nevertheless, embrittlement ensued as the MWCNTs content increases to above 3 wt % (Figure 6). On the basis of the analyses above, the embrittlement was owing to the increased difficulty of craze initiation and the subsequent growth that follows the initiation. The local strain and stress within the incipient crazes, as shown in Figure 3, parts a and b, for $c_o = 2$ wt %, increased with $c_o$ such that craze initiation would eventually be suppressed. When fewer crazes were available to absorb the deformation energy, cracking ultimately became preferentially favored.

**Straining of MWCNTs within SDZs.** With straight and sharp boundaries under an optical microscope, SDZs nucleated in the neat PPO films at approximately $\epsilon = 2\%$. They widened steadily as strain increased and eventually broke down to form cracks for $\epsilon > 13\%$ (Figure 7a). Before voids were initiated, however, the SDZ could grow to a width as wide as 40 $\mu$m. The depth $d$ of the SDZs, measured by AFM, followed a typical micronecking characteristic in that $d$ increased linearly with $w$ up to $w = w_c$, thereafter leveling to a constant depression (Figure 8a). The SDZs were generally smooth, under the TEM, with some secondary wavy striations lying perpendicular to the stretching direction.

The morphology of the SDZs underwent large changes when a small amount of MWCNTs was added into the polymer matrix. For $c_0$'s as small as 1.5 wt %, the SDZs had become short and narrow ($w < 8$ $\mu$m), more numerous, and the film remained intact for $\epsilon$'s up to ~16% (Figure 7b). These effects are quite similar to that observed in MWCNTs/PS systems where strain delocalization had modified the nanoplastic flow behavior. However, these SDZs manifested very different interactions with the embedded MWCNTs, as compared to crazes, in that the MWCNTs were found to draw into the SDZs regardless of the zone width, as revealed under TEM (Figure 7, parts c and d). The incorporated MWCNTs were either perfectly straightened along the drawing direction (for smaller diameters, ca. > 20 nm, Figure 7c), or aligned to a lesser degree but with obvious local debonding taking place at the interfaces with the polymer matrix (for these MWCNTs of greater diameters, Figures 7d). Clearly, there is no pileup of MWCNTs at the boundaries of the deformation zones. Consistent with this observation, the AFM topography of the mildly etched SDZ also did not show any protrusions at the zone edges (Figure 8b). It is thus obvious that the MWCNTs can be drawn by the nanoplastic flow into the SDZs.

The incorporation of the MWCNTs in the nanoplastic flow, furthermore, produced an accelerated strain hardening of the flow in that the leveling depression $d_s$ decreased as $c_0$ increased (Figure 8, parts a and e). It decreased from 0.26, of the original thickness for the neat resin, to 0.13, for $c_o = 2.4$ wt % (Figure 8a). Since the draw ratio ($\lambda_{SDZ}$) in the SDZs scales very closely with the leveling depression $d_s$ via $\lambda_{SDZ} \sim \tau_0/(\tau_0 - 2d_s)$,[22–25,27,30–32] The decrease of ($d_s/\tau_0$) from 0.26 to 0.13 for a change from $c_o = 0$ to $c_o = 2.4\%$ translates into a decrease of

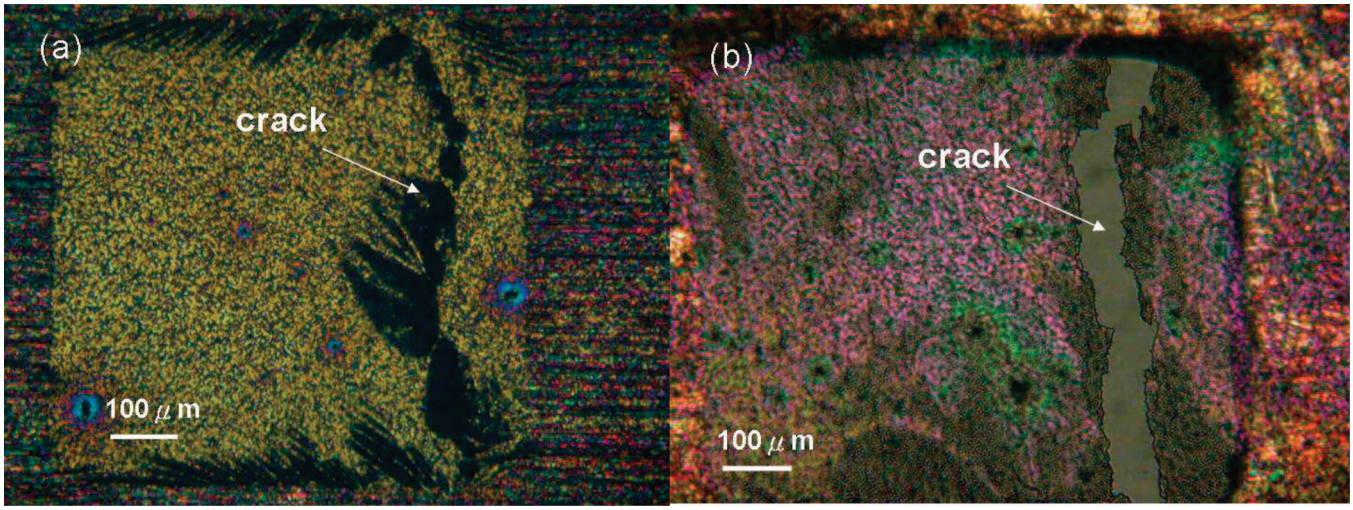


**Figure 6.** Optical micrographs of stretched MWCNT/PS films at high MWCNTs content: (a) 3 and (b) 5 wt %.

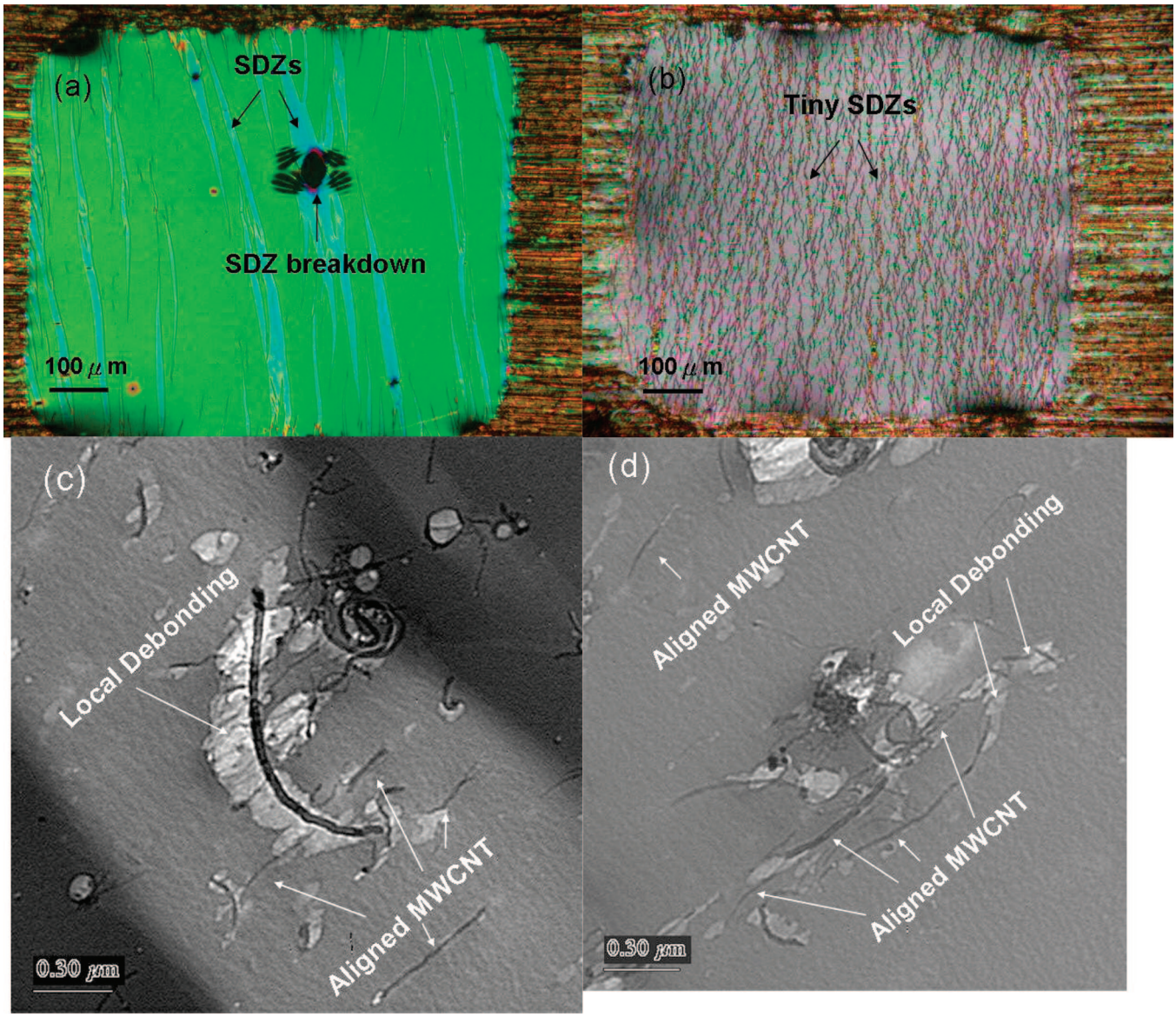


**Figure 7.** Optical micrographs of stretched (a) pristine PPO films, (b) MWCNTs/PPO composite film (weight fraction of MWCNT is 1.5 wt %), and (c) TEM micrographs of narrow SDZ, and (d) TEM micrograph of a wider SDZ in MWCNT/PPO films ($c_0$ = 1.5 wt %).

$\lambda_{SDZ}$ from 2.08 to 1.35, a 3-fold decrease of the molecular strain. This, however, is consistent with the fact that the volume fractions of MWCNTs ($c_o$'s) are already significantly greater than the percolation threshold of MWCNTs, approximately 0.08 vol %, for the MWCNTs. The slope of the linear increase of $d$ versus $w$ during the initial necking also decreases with $c_o$, indicating an increase of chain friction in the PPO/MWCNTs nanocomposites.

The increase of chain friction of the nanoplastic flow in MWCNTs/PPO was estimated by use of the Rouse chains model as applied for crazes in the PS systems before with $A_{chain}$ of the PPO chain approximately 0.55 nm$^2$. For both the pristine PPO and MWCNTs/PPO films, the tube sliding velocities $v$'s, measured from SDZ widening, were shown, with somewhat large data fluctuations, to be indistinguishable from each other; they were almost constant ($\sim$ 1500 nm/s) but in fact slowly decrease with $w$ (Figure 8c). The friction coefficient $\zeta_T$ was found to increase with the $w$ when $w < w_c$ but then began leveling-off for $w > w_c$ (Figure 8d). The addition of the MWCNTs (1.5wt.%) in PPO had raised the chain friction from $\zeta_{PPO} \sim 4.3 \times 10^{-5}$ kg/s to $\zeta_T \sim 7.5 \times 10^{-5}$ kg/s, but the overall trend remains unchanged. Clearly, the incorporation of MWCNTs during the nanoplastic flow had dramatically reduced the extensibility of the entanglement network of the PPO matrix.

**Strain-Hardening of the Entangled Chains.** The intriguing differences between SDZs and crazes in the interactions with MWCNTs obviously should be related to the plastic flow properties of the entanglement network incurred during the local deformation. According to Kramer,[22–25,27,30–32] the state of deformation induced by the deformation zones is related to the structure of entanglement network. For example, the average draw ratio of the plastic flow, $\lambda_{craze}$ or $\lambda_{SDZ}$, scales approximately with the extensibility of the chain network, $\lambda_{max}$, defined as $\lambda_{max} l_e/d_e$ where $l_e$ is the contour length between entanglements and $d_e$ is the direct distance between them.[22–25,27,30–32] The PPO is known to has a tighter entanglement chain network ($\lambda_{max}$ = 3.1, $\nu_e = 1.5 \times 10^{26}$ chains/m$^3$) compared to that of PS ($\lambda$ = 4.2, $\nu_e = 3.3 \times 10^{25}$ chains/m$^3$) (shown schematically in Figure 9a).[22,32] Furthermore, the deformations of the entanglement networks in both PS and PPO had been explored before by microscopic stress analyses from the AFM topography.[33–35,37–39] It was found that both entanglement networks manifested a two-stage process, strain-softening and strain-hardening, during the

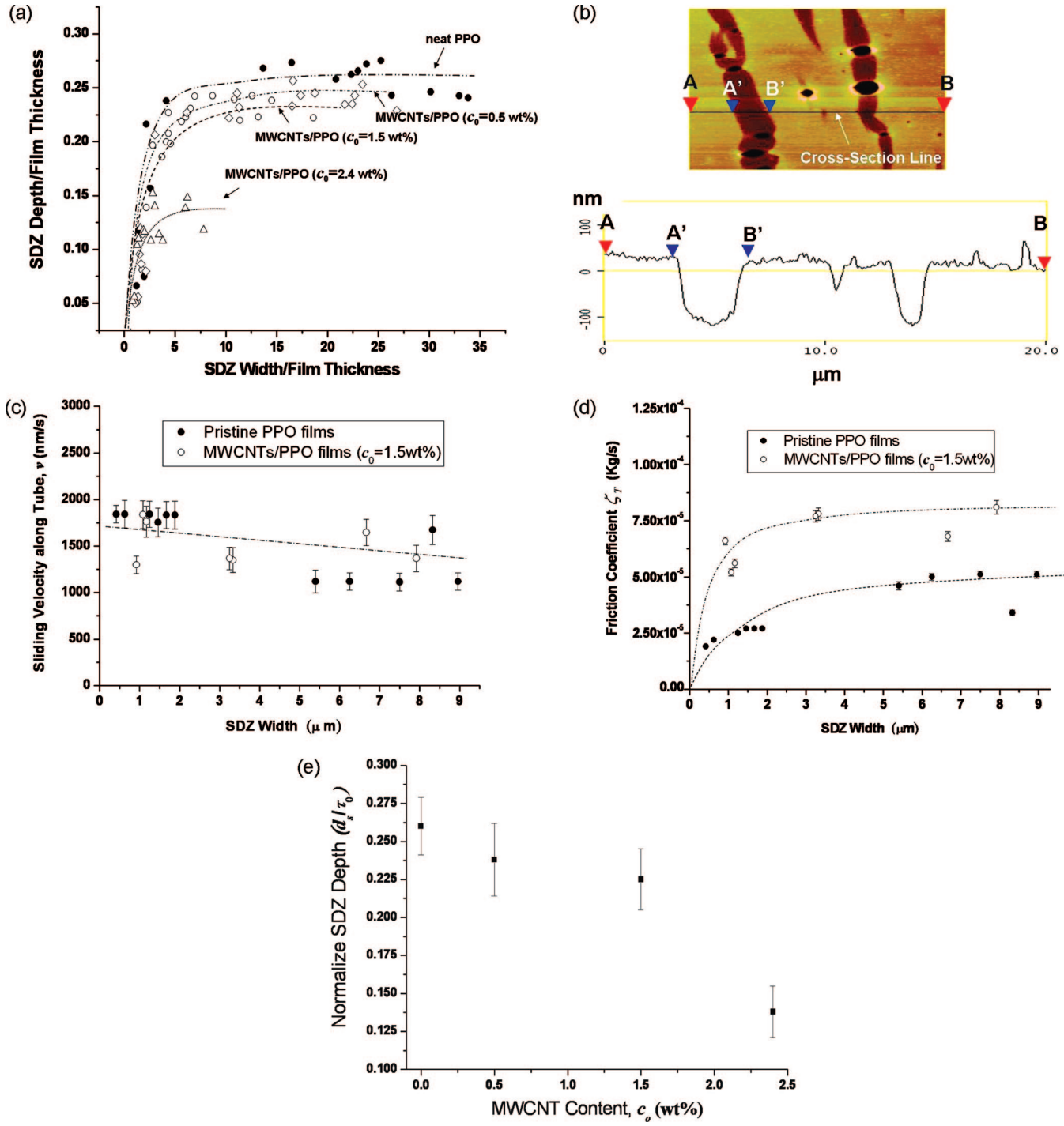


**Figure 8.** (a) SDZ depth vs SDZ width in the pristine PPO and MWNTs/PPO films: pristine PPO films ($c_0 = 0$ wt %) (ζ, $c_0 = 2.4$ wt % (ζ, $c_0 =$ 1.5 wt % (ζ; $c_0 = 0.5$ wt % (ζ). (b) AFM micrographs of the stretched and etched MWNTs/PPO films. (c) Tube sliding velocity of a PPO chain versus SDZ width in pristine PPO and MWCNT/PPO films, (d) Friction coefficient of a PPO chain versus SDZ width in pristine PPO and MWCNT/PPO films. (e) Normalized SDZ depth versus $c_0$.

deformation with a critical strain $\epsilon_h$ (dubbed as the hardening strain) dividing these two regimes.[34,37] The hardening strains $\epsilon_h$'s for crazing in the loose chain network of PS and that for SDZs in the tighter PPO chain network were quite different. The hardening strain $\epsilon_h$ of PS (of molar mass 2M) was determined to be $\epsilon_h = 1.4$ while it was approximately $\epsilon_h = 0.3$ for PPO.[34]

With this, the drawing mechanics of the plastic flows were further analyzed by comparing $\epsilon_h$'s of the two polymers with the corresponding maximum strain $\epsilon_p$'s (the plateau strain) in the films (Figure 9b). Although the plateau strains $\epsilon_p$'s for both PS and PPO increase monotonically with $w$, the plateau strains $\epsilon_p$'s for $w < 5$ $\mu$m in MWCNTs/PS were smaller than the hardening strain ($\epsilon = 1.4$) of the PS chain network. Recalling that virtually all the crazes formed in the MWCNTs/PS films were thinner than 2 $\mu$m in width, it indicates that the PS chains in the nanoplastic flows were still in the strain-softening stage, incapable of drawing the relatively much more rigid MWCNTs into crazes. On the contrary, the plateau strains $\epsilon_p$'s in the SDZs of MWCNTs/PPO would be greater than $\epsilon_h$ of the PPO chain network ($\epsilon = 0.3$) for $w > 0.6$ $\mu$m. Since most SDZs in the MWCNTs/PPO nanocomposite were wider than that (0.6 $\mu$m),

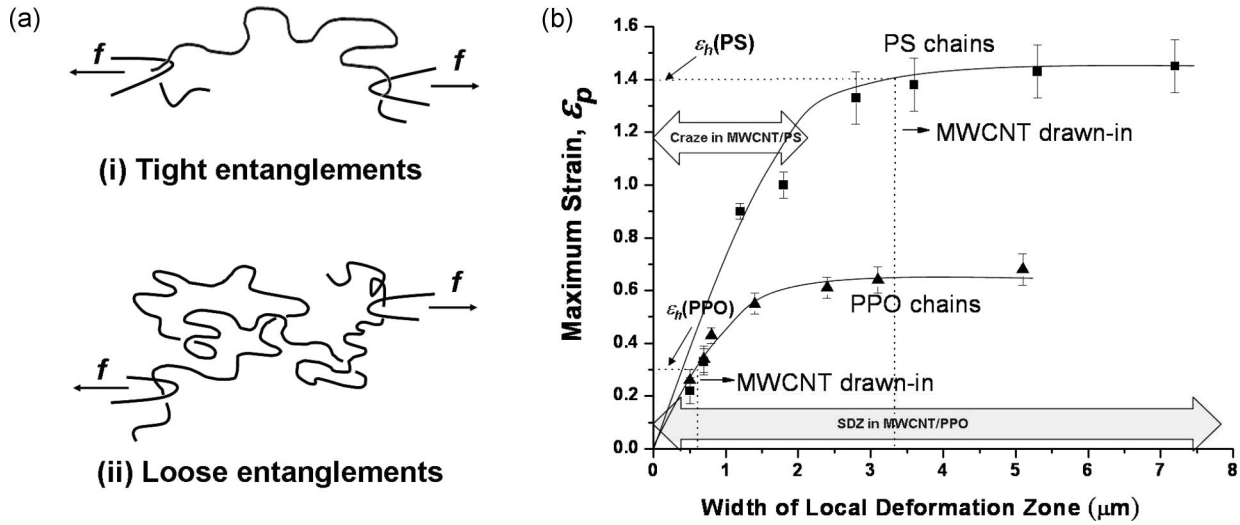


**Figure 9.** (a) Schematic drawings of tight and loose chain entanglements, and (b) the local maximum strain versus the width of local deformation zones.

the PPO chains in the nanoplastic flow were able to pull the MWCNTs into the local deformation zones.

## Discussions

The length scales of interactions during the drawing of surface grafted MWCNTs by the nanoplastic flows of glassy polymers may be in the order of tens of nanometers, as hinted by the diameter of MWCNTs (~25 nm), due to the fact that some degrees of local bending of the MWCNTs obviously deemed inevitable. Since the bending moment of CNTs increases approximately to the third power of the tube diameter, drawing of CNTs would become more dominant, as opposed to polymer draining through the CNTs, during the nanoplastic flows when the diameter of the CNTs decreases. Early results seems to confirm this picture in that single-walled CNTs (SWCNTs) were observed being drawn into crazes in films of the bulky polybenzoxazoles macromolecules where SWCNTs were surface treated by a physical adsorption means.[49]

In the light of this, other than the improved compatibility that has led to uniform dispersion of CNTs in the polymer matrix, the effects of molecular weight and the amount of the grafted polymers[50] may be primarily on the magnitude of tube friction $\zeta_T$ during the nanoplastic flows. Higher molecular weights and greater polymer fractions are expected to increase the frictions. It, however, would not qualitatively alter the major observations obtained in this experiment. Further explorations in this direction is interesting but is beyond the scope of this study.

The range of CNT fractions (0−10 wt %) explored in this experiment covers the regime (>0.1 wt %) where the dispersed CNTs percolate electrically.[49] However, electric percolation does not correspond to mechanical percolation where the CNTs would effectively form a network that is fully stress-bearing. As revealed by the PS systems, CNT displacement that causes substantial modifications of the purported CNTs network occurs upon stretching as polymer chains draining through the CNTs to cause local CNT pileup at the craze boundaries. In the strain-hardening system of PPO, although the CNTs can be drawn into the SDZs, they at the same time did not escape the fate of strain localization and underwent fracture at a strain not significantly greater than those without them. Apparently, control over the state of entanglement between CNTs and stability of the CNTs network requires further material engineering that exploits the properties and geometries of individual CNTs as well as nanostructuring them into right space. The notion of a stress-bearing entanglement network of CNTs that effectively shield the polymer composite from mechanical stress remains to be tested by further experiments and is out of the scope of the intended study here. For the range of very dilute CNT fractions (>1 wt %), the effect on the nanoplastic flow is minute, however.

With the micromechanical analyses based on AFM data, the interactions between the embedded MWCNTs and the glassy polymer chains during the nanoplastic flows can be understood in a simple and coherent framework in terms of the plastic flows micromechanics and the properties/structure of the chain entanglement network. The complicated effects of filler arising from MWCNTs in glassy polymers can be understood further by pursuits using this approach. The important fundamental behavior of glassy polymer chain during the nanoplastic flows of crazing or shear yielding can be unveiled with advances of the chain-MWCNTs interactions.

## Conclusions

In conclusion, the surface-grafted MWCNTs dispersed in a polymer matrix dramatically toughen the glassy polymer by delocalization of plastic flows, engendered by a significant increase of chain friction during microdeformation. The interactions between the MWCNTs and polymer chains, however, are quite different for craze-forming brittle polymer (PS) and SDZ-forming ductile polymer (PPO), which can be attributed to variations in the chain entanglement network structure. For PS, the CNTs-polymer interactions during the plastic flow is in the regime of polymer strain softening in which the polymer chains drawn into crazes are filtering through the pileup of MWCNTs at craze boundaries. The pileup is resulted from the incapability of the softened chains to pull the rigid CNTs into the nanoplastic flow. In this situation, chain friction increases linearly with craze width during widening of the craze and ultimately forces nucleation of new crazes, leading to delocalization of the strain. In contrast, the PPO chains undergo strain-hardeing during the nanoplastic flow and are capable to draw MWCNTs into the SDZs, leaving no pileup of MWCNTs at the zone boundaries. The delocalization effect due to MWCNTs is thus much smaller as compared to that in MWCNTS/PS and the SDZs can still grow to a width significantly wider than crazes in PS/MWCNTs of the same MWCNTs loadings. The physical participation of MWCNTs in the nanoplastic flows of PPO has generated an

increase of chain friction although it does not alter qualitatively the dependence of chain friction on the degree of drawing during the flow. The incorporation of MWCNTs in the flow considerably reduce the extensibility of the glassy polymer, giving rise to substantially lower plateau strain of the plastic flow (3 time reduction for $c_0 = 2.4$ wt %) and higher draw stress (1.5 time increase for $c_0 = 2.4$ wt %). At high MWCNTs contents in either PS or PPO, the increase of chain friction eventually suppresses the formation of crazes or SDZs and ultimately leads to embrittlement of the nanocomposites.

**Acknowledgment.** We greatly appreciate the financial support of National Science Council of Taiwan and grants from the US Air Force Office of Scientific Research (AOARD-044074/AOARD-064067) through the Taiwan−US Air Force Nanoscience Initiative Program.

## References and Notes

(1) Yu, M. F.; Lourie, O.; Dyer, M. J.; Moloni, K.; Kelly, T. F.; Ruoff, R. S. *Science* **2000**, *287*, 637.
(2) Hwang, G. L.; Hwang, K. C. *Nano Lett.* **2001**, *1*, 435.
(3) Bekyarova, E.; Itkis, M. E.; Cabrera, N.; Zhao, B.; Yu, A.; Gao, J.; Haddon, R. C. *J. Am. Chem. Soc.* **2005**, *127*, 5990.
(4) Hecht, D.; Hu, L.; Gruner, G. *Appl. Phys. Lett.* **2006**, *89*, 133112.
(5) Yakobson, B. I.; Campbell, M. P.; Brabec, C. J.; Bernholc, J. *Comput. Mater. Sci.* **1997**, *8*, 341.
(6) Yang, Y.; Gupta, M. C.; Dudley, K. L.; Lawrence, R. W. *Nano Lett.* **2001**, *5*, 2131.
(7) Hill, D. E.; Lin, Y.; Rao, A. M.; Allard, L. F.; Sun, Y. P. *Macromol.* **2002**, *35*, 9466.
(8) Liu, C. H.; Fan, S. S. *Appl. Phys. Lett.* **2005**, *86*, 123106–1.
(9) Qian, D.; Dickey, E. C. *Appl. Phys. Lett.* **2000**, *76*, 2868.
(10) Blond, D; Barron, V.; Ruether, M.; Ryan, K. P.; Nicolosi, V.; Blau, W. J.; Coleman, J. N. *Adv. Funct. Mater* **2006**, *16*, 1608.
(11) Hwang, G. L.; Shieh, Y. T.; Hwang, K. C *Adv. Funct. Mater.* **2004**, *14*, 487.
(12) Coleman, J. N.; Cadek, M.; Blake, R.; Nicolosi, V.; Ryan, K. P.; Belton, C.; Fonseca, A.; Nagy, J. B.; Gun'ko, Y. K.; Blau, W. J. *Adv. Funct. Mater.* **2004**, *14*, 791.
(13) Singh, S.; Pei, Y.; Miller, R.; Sundararajan, P, R. *Adv. Funct. Mater* **2003**, *13*, 868.
(14) Zhu, J.; Kim, J.; Peng, H.; Margrave, J. L.; Khabashesku, V. N.; Barrera, E. V. *Nano Lett.* **2003**, *3*, 1107.
(15) Li, X.; Gao, H.; Scrivens, W. A.; Fei, D.; Xu, Xiaoyou; Sutton, M. A.; Reynolds, A. P.; Myrick, M. L. *Nanotech* **2004**, *15*, 1416.
(16) Qian, D.; Dickey, E. C. *J. Micro.* **2001**, *204*, 39.
(17) Watts, P. C. P.; Hsu, W. K. *Nanotech* **2003**, *14*, L7.
(18) Liu, T. X.; Phang, I. Y.; Shen, L.; Chow, S. Y.; Zhang, W. D. *Macromolecules* **2004**, *37*, 7214.
(19) Zhang, W. D.; Shen, L.; Phang, I. Y.; Liu, T. X. *Macromolecules* **2004**, *37*, 256.
(20) Manchado, M. A.; Valetini, L.; Biagiotti, J.; Kenny, J. M. *Carbon* **2005**, *43*, 1499.
(21) Meincke, O.; Kaempfer, D.; Weickmann, H.; Friedrich, C.; Vathauer, M.; Warth, H. *Polymer* **2004**, *45*, 739.
(22) Kramer, E. J. *Adv. Polym. Sci.* **1983**, *52/53*, 1.
(23) Donald, A. M.; Kramer, E. J *J. Polym. Sci.: Polym. Phys.* **1982**, *20*, 899.
(24) Donald, A. M.; Kramer, E. J *J. Polym. Sci.: Polym. Phys.* **1982**, *23*, 1183.
(25) Donald, A. M.; Kramer, E. J. *Polymer* **1982**, *23*, 461.
(26) Donald, A. M.; Kramer, E. J. *Polymer* **1982**, *23*, 457.
(27) Henkee, C. S.; Kramer, E. J. *J. Polym. Sci.: Polym. Phys.* **1985**, *22*, 721.
(28) Yang, A. C.-M.; Kramer, E. J. *J. Polym. Sci.: Polym.Phys* **1985**, *23*, 1353.
(29) Yang, A. C.-M.; Kramer, E. J. *J. Mater. Sci.* **1986**, *21*, 3601.
(30) Yang, A. C. M.; Kramer, E. J.; Kuo, C. C.; Phoenix, S. L. *Macromolecules* **1986**, *19*, 2010.
(31) Yang, A. C. M.; Kramer, E. J.; Kuo, C. C.; Phoenix, S. L. *Macromolecules* **1986**, *19*, 2020.
(32) Kramer, E. J.; Berger, L. L. *Adv. Polym. Sci.* **1990**, *91/92*, 1.
(33) Yang, A. C. M.; Kunz, M. S.; Logan, J. A. *Macromolecules* **1993**, *26*, 1776.
(34) Lin, J. H.; Yang, A. C. M. *Macromolecules* **2001**, *34*, 3698.
(35) Lin, C. H.; Yang, A. C. M. *Macromolecules* **2001**, *34*, 4865.
(36) Yang, A. C. M; Wang, R. C.; Lin, J. H. *Polymer* **1996**, *37*, 5751.
(37) Yang, A. C.-M.; Wang, R. C.; Kunz, M. S.; Yang, I. C. *J. Polym. Sci.: Polym. Phys. Ed.* **1996**, *34*, 1141.
(38) Hsiao, C. C.; Lin, T. S.; Cheng, L. Y.; Ma, C. C. M.; Yang, A. C. M. *Macromolecules* **2005**, *38*, 4811.
(39) Lin, T. S.; Cheng, L. Y.; Hsiao, C. C.; Yang, A. C. M. *Mater. Chem. Phys.* **2005**, *94*, 438.
(40) Kong, H.; Gao, C.; Yan, D. *Macromolecules* **2004**, *37*, 4022.
(41) Bridgman, D. W. *Studies in Large Plastic Flow and Fracture*; Harvard University Press: Cambridge, U.K., 1964: p 9.
(42) Hutchinson, J. W.; Neale, K. W. *J. Mech. Phys. Solids* **1983**, *31*, 405.
(43) G'sell, C.; Marquez-Lucero, A. *Polymer* **1993**, *34*, 2740.
(44) Rubinstein, M.; Colby, R. H. *Polymer Physics*,Oxford University Press, Oxford, 2003; Chapter 9.
(45) The area of the confining tube ($A_{chain}$) for a single PS chain was calculated by $A_{chain} = M_0/(N_{Av}\rho b)$ where $M_0$ is the molar mass of a Kuhn monomer, $N_{Av}$ is Avogadro's number, $\rho$ is the density, and $b$ is the Kuhn length.
(46) A polymer segment in the wormlike tube has to move a contour length of $l = bN$ to produce a translational distance of $R = bN^{1/2}$. Therefore, the sliding velocity within the tube is $N^{1/2}$ times the linear velocity measured from deformation zone widening.
(47) Cotiuga, I.; Picchioni, F.; Agarwal, U. S.; Wouters, D.; Loos, J.; Lemstra, P. *Macromol. Rapid Commun.* **2006**, *27*, 1073.
(48) Doi, M.; Edward, S. F. *The Theory of Polymer Dynamics*; Clarendon: Oxford, U.K., 1986; p 338.
(49) Yang, A. C.-M. Micro-mechanisms of deformation, conduction percolation and nanotube crosslinking via surface grafting polymerization in CNT-polymer nanocomposites. The 4th US Air Force−Taiwan Nanoscience Initiative Workshop, University of Houston, Houston, TX, Feburary 8−9, 2007.
(50) Lee, J. Y.; Zhang, Q.; Emrick, T.; Crosby, A. J. *Macromolecules* **2006**, *39*, 7392.

MA702342Z